

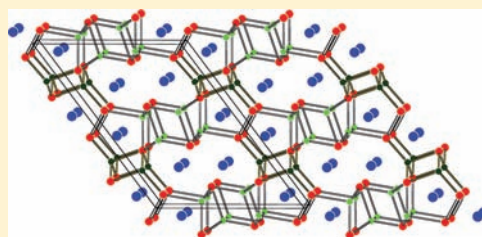
Ternary Arsenides  $A_2Zn_2As_3$  ( $A = Sr, Eu$ ) and Their Stuffed Derivatives  $A_2Ag_2ZnAs_3$ 

Stanislav S. Stoyko, Mansura Khatun, and Arthur Mar\*

Department of Chemistry, University of Alberta, Edmonton, Alberta, Canada T6G 2G2

## Supporting Information

**ABSTRACT:** The ternary arsenides  $A_2Zn_2As_3$  and the quaternary derivatives  $A_2Ag_2ZnAs_3$  ( $A = Sr, Eu$ ) have been prepared by stoichiometric reaction of the elements at 800 °C. Compounds  $A_2Zn_2As_3$  crystallize with the monoclinic  $Ba_2Cd_2Sb_3$ -type structure (Pearson symbol  $mC28$ , space group  $C2/m$ ,  $Z = 4$ ;  $a = 16.212(5)$  Å,  $b = 4.275(1)$  Å,  $c = 11.955(3)$  Å,  $\beta = 126.271(3)^\circ$  for  $Sr_2Zn_2As_3$ ;  $a = 16.032(4)$  Å,  $b = 4.255(1)$  Å,  $c = 11.871(3)$  Å,  $\beta = 126.525(3)^\circ$  for  $Eu_2Zn_2As_3$ ) in which  $CaAl_2Si_2$ -type fragments, built up of edge-sharing Zn-centered tetrahedra, are interconnected by homoatomic As–As bonds to form anionic slabs  $[Zn_2As_3]^{4-}$  separated by  $A^{2+}$  cations. Compounds  $A_2Ag_2ZnAs_3$  crystallize with the monoclinic  $Yb_2Zn_3Ge_3$ -type structure (Pearson symbol  $mC32$ , space group  $C2/m$ ;  $a = 16.759(2)$  Å,  $b = 4.4689(5)$  Å,  $c = 12.202(1)$  Å,  $\beta = 127.058(1)^\circ$  for  $Sr_2Ag_2ZnAs_3$ ;  $a = 16.427(1)$  Å,  $b = 4.4721(3)$  Å,  $c = 11.9613(7)$  Å,  $\beta = 126.205(1)^\circ$  for  $Eu_2Ag_2ZnAs_3$ ), which can be regarded as a stuffed derivative of the  $Ba_2Cd_2Sb_3$ -type structure with additional transition-metal atoms in tetrahedral coordination inserted to link the anionic slabs together. The Ag and Zn atoms undergo disorder but with preferential occupancy over four sites centered in either tetrahedral or trigonal planar geometry. The site distribution of these metal atoms depends on a complex interplay of size and electronic factors. All compounds are Zintl phases. Band structure calculations predict that  $Sr_2Zn_2As_3$  is a narrow band gap semiconductor and  $Sr_2Ag_2ZnAs_3$  is a semimetal. Electrical resistivity measurements revealed band gaps of 0.04 eV for  $Sr_2Zn_2As_3$  and 0.02 eV for  $Eu_2Zn_2As_3$ , the latter undergoing an apparent metal-to-semiconductor transition at 25 K.



## INTRODUCTION

Many ternary pnictides  $A-M-Pn$  (where  $A$  is a divalent electropositive metal (Ca, Sr, Ba, Eu, Yb),  $M$  is a transition metal, and  $Pn = P, As, Sb, Bi$ ) can be regarded as Zintl phases. Antimonide representatives such as  $AZn_2Sb_2$  and  $Yb_{14}MnSb_{11}$  are promising thermoelectric materials by virtue of their narrow band gaps (associated with the charge-balanced formulations in Zintl phases), their complex crystal structures, and the presence of heavy elements.<sup>1,2</sup> Arsenide representatives such as those based on the parent compound  $BaFe_2As_2$  are superconductors with relatively high critical temperatures, although here there is no gap at the Fermi level and the electronic structure is quite amenable to modification through doping.<sup>3–5</sup>

The ternary Zn- and Cd-containing arsenides in these systems are particularly numerous:  $AZn_2As_2$  and  $ACd_2As_2$  ( $A = Ca, Sr, Ba, Eu, Yb$ ) with the  $CaAl_2Si_2$ -type structure are the most prevalent phases,<sup>6–13</sup>  $BaZn_2As_2$  has two polymorphs,<sup>14,15</sup>  $A_2ZnAs_2$  ( $A = Sr, Ba, Eu$ ) and  $A_2CdAs_2$  ( $A = Ca, Sr, Ba, Eu$ ) crystallize in several polymorphic forms,<sup>16–18</sup>  $Eu_{11}Zn_6As_{12}$  adopts the  $Sr_{11}Cd_6Sb_{12}$ -type structure,<sup>19</sup> and  $Ba_2Cd_2As_3$  is a recently reported phase with a structure closely related to the  $CaAl_2Si_2$  type.<sup>20</sup> The latter compound supports mixing of the cation or anion sites to give the members of solid solution  $(Ba_{1-x}Sr_x)Cd_2As_3$  or  $Ba_2Cd_2(As_{1-x}Sb_x)_3$ , respectively.<sup>20</sup> However, substitution of the transition-metal component remains unexplored.

We present here the preparation of  $Sr_2Zn_2As_3$  and  $Eu_2Zn_2As_3$ , which are new representatives of the  $Ba_2Cd_2As_3$ -type structure. Investigation of the extent of transition-metal substitution in this series has led to the discovery of the isoelectronic quaternary derivatives  $Sr_2Ag_2ZnAs_3$  and  $Eu_2Ag_2ZnAs_3$  in which Ag atoms are stuffed into the ternary host structures. Their electronic structures were examined through band structure calculations and electrical resistivity measurements.

## EXPERIMENTAL SECTION

**Synthesis.**  $Eu_2Zn_2As_3$  was first identified in the course of systematic investigations of ternary rare-earth arsenide systems  $RE-Zn-As$  in which  $REZn_{1-x}As_2$  and  $REZn_3As_3$  phases are formed for the earlier  $RE$  metals.<sup>21–23</sup> Substitution of Eu with Sr led to formation of the isostructural compound  $Sr_2Zn_2As_3$ . Starting materials were Eu pieces (99.99%, Hefa), Sr pieces (99.8%, Alfa-Aesar), Zn shot (99.99%, Aldrich), Ag powder (99.99%, Aldrich), and As lumps (99.999%, Alfa-Aesar). All reagents and products were handled within an argon-filled glovebox. The surfaces of the Eu and Sr pieces were scraped clean with a scalpel. Mixtures of the elements in the molar ratio  $A:Zn:As = 2:2:3$  and  $A:Ag:Zn:As = 2:2:1:3$  were loaded into alumina crucibles placed within fused silica tubes, which were evacuated and sealed. The tubes were heated to 850 °C over

Received: November 30, 2011

Published: January 24, 2012

Table 1. Crystallographic Data for  $A_2Zn_2As_3$  and  $A_2Ag_2ZnAs_3$  (A = Sr, Eu)

formula	$Sr_2Zn_2As_3$	$Eu_2Zn_2As_3$	$Sr_2Ag_{1.99(2)}Zn_{1.00(3)}As_3$	$Eu_2Ag_{2.03(2)}Zn_{0.98(3)}As_{3.08(1)}$
formula mass (amu)	530.74	659.42	681.11	816.47
space group	$C2/m$ (No. 12)	$C2/m$ (No. 12)	$C2/m$ (No. 12)	$C2/m$ (No. 12)
<i>a</i> (Å)	16.212(5)	16.032(4)	16.759(2)	16.427(1)
<i>b</i> (Å)	4.275(1)	4.255(1)	4.4689(5)	4.4721(3)
<i>c</i> (Å)	11.955(3)	11.871(3)	12.202(1)	11.9613(7)
$\beta$ (deg)	126.271(3)	126.525(3)	127.058(1)	126.205(1)
<i>V</i> (Å <sup>3</sup> )	668.1(3)	650.8(3)	729.3(1)	709.03(8)
<i>Z</i>	4	4	4	4
$\rho_{\text{calcd}}$ (g cm <sup>-3</sup> )	5.277	6.731	6.204	7.649
<i>T</i> (K)	173(2)	173(2)	173(2)	173(2)
cryst dimens (mm)	0.02 × 0.04 × 0.39	0.02 × 0.03 × 0.51	0.07 × 0.09 × 0.32	0.07 × 0.08 × 0.17
radiation	graphite-monochromated Mo $K\alpha$ , $\lambda = 0.71073$ Å			
$\mu$ (Mo $K\alpha$ ) (mm <sup>-1</sup> )	37.59	41.29	36.44	40.30
transmission factors	0.055–0.652	0.042–0.537	0.017–0.174	0.044–0.167
2 $\theta$ limits, deg	4.22–66.08	4.26–66.12	4.18–66.50	4.22–66.42
data collected	$-24 \leq h \leq 23$ $-6 \leq k \leq 6$ $-17 \leq l \leq 17$	$-24 \leq h \leq 24$ $-6 \leq k \leq 6$ $-18 \leq l \leq 18$	$-25 \leq h \leq 25$ $-6 \leq k \leq 6$ $-36 \leq l \leq 36$	$-24 \leq h \leq 25$ $-6 \leq k \leq 6$ $-18 \leq l \leq 17$
no. of data collected	4595	4487	5042	4900
no. of unique data, including $F_o^2 < 0$	1374 ( $R_{\text{int}} = 0.031$ )	1333 ( $R_{\text{int}} = 0.030$ )	1502 ( $R_{\text{int}} = 0.019$ )	1458 ( $R_{\text{int}} = 0.028$ )
no. of unique data, with $F_o^2 > 2\sigma(F_o^2)$	1171	1172	1430	1410
no. of variables	44	44	59	61
$R(F)$ for $F_o^2 > 2\sigma(F_o^2)^a$	0.022	0.019	0.027	0.031
$R_w(F_o^2)^b$	0.046	0.037	0.059	0.072
goodness of fit	1.04	1.01	1.10	1.10
$(\Delta\rho)_{\text{max}}$ ( $\Delta\rho)_{\text{min}}$ (e Å <sup>-3</sup> )	1.32, -0.99	1.53, -1.32	4.74, -3.19	6.61, -4.71

$$^a R(F) = \sum ||F_o| - |F_c|| / \sum |F_o|. \quad ^b R_w(F_o^2) = [\sum [w(F_o^2 - F_c^2)^2] / \sum wF_o^4]^{1/2}; \quad w^{-1} = [\sigma^2(F_o^2) + (Ap)^2 + Bp], \quad \text{where } p = [\max(F_o^2, 0) + 2F_c^2] / 3.$$

2 days, kept at that temperature for 1 day, cooled to 800 °C over 1 day, kept at that temperature for 7 days, and cooled to room temperature over 2 days. Products were analyzed by powder X-ray diffraction (XRD) on a Si-calibrated Inel diffractometer equipped with a curved position-sensitive detector (CPS 120) and a Cu  $K\alpha_1$  radiation source operated at 40 kV and 20 mA. The powder XRD patterns revealed that the products contained  $A_2Zn_2As_3$  or  $A_2Ag_2ZnAs_3$  as the major phase (60–90%) with smaller amounts of other ternary arsenides, usually  $AZn_2As_2$  (Figures S1 and S2 in Supporting Information). The heat treatments above also yielded gray needle-shaped crystals of the title compounds (Figure S3 in Supporting Information), which were examined by energy-dispersive X-ray (EDX) analysis on a Zeiss EVO MA 15 scanning electron microscope. The average compositions (in atomic %) determined over 5–6 crystals per sample ( $Sr_{2.9(1)}Zn_{2.6(1)}As_{4.5(2)}$ ,  $Eu_{2.8(1)}Zn_{2.9(1)}As_{4.3(2)}$ ,  $Sr_{2.5(1)}Ag_{2.6(1)}Zn_{1.3(1)}As_{3.6(2)}$ ,  $Eu_{2.4(1)}Ag_{2.7(1)}Zn_{1.1(1)}As_{3.8(2)}$ ) were in good agreement with the expected compositions ( $A_{2.8,6}Zn_{2.8,6}As_{4.2,8}$  and  $A_{2.5,0}Ag_{2.5,0}Zn_{1.2,5}As_{3.7,5}$ ). These crystals are moisture air stable, their surfaces tarnishing within several days.

**Structure Determination.** Suitable single crystals of  $A_2Zn_2As_3$  and  $A_2Ag_2ZnAs_3$  were selected from crushed samples examined under paraffin oil. They were mounted on glass fibers under a cold nitrogen gas stream on a Bruker D8/SMART APEX II diffractometer equipped with a Mo  $K\alpha$  radiation source. Full spheres of intensity data were collected at -100 °C using  $\omega$  scans with a scan width of 0.3° and an exposure time of 15 s per frame in 5 batches. Face-indexed numerical absorption corrections were applied. Structure solution and refinement were carried out with the use of the SHELXTL (version 6.12)

program package.<sup>24</sup> Crystal data and further experimental details are given in Table 1.

For  $A_2Zn_2As_3$ , the centrosymmetric monoclinic space group  $C2/m$  was chosen on the basis of the Laue symmetry, systematic absences, and intensity statistics (mean  $|E^2 - 1|$  of 1.026 for  $Sr_2Zn_2As_3$  and 0.958 for  $Eu_2Zn_2As_3$ ). Initial atomic positions were easily located by direct methods, and refinements proceeded without complications. All sites are fully occupied and have reasonable displacement parameters.

For  $A_2Ag_2ZnAs_3$ , structure determinations were less straightforward. The space group  $C2/m$  was also most appropriate based on intensity statistics (mean  $|E^2 - 1|$  of 0.968 for  $Sr_2Ag_2ZnAs_3$  and 0.872 for  $Eu_2Ag_2ZnAs_3$ ). The similarity of the monoclinic cell parameters to those of  $A_2Zn_2As_3$  suggests close structural relationships. Direct methods revealed sites at close to the same locations as in  $A_2Zn_2As_3$ , except that there is a third site for the transition-metal atoms (labeled as M3), and the Zn1 site is now split into two separated by 0.5 Å (labeled as M1a and M1b). Disorder of the Ag and Zn atoms over the three transition-metal sites was treated by introducing several restraints: (i) the sum of the occupancies in each of the M2 or M3 sites is unity, (ii) the sum of the occupancies of the M1a and M1b sites together is unity, and their displacement parameters are constrained to be equal, and (iii) the sum of the charges ( $Ag^+$ ,  $Zn^{2+}$ ) over all these sites is 4+ per formula unit. For the Sr-containing crystal, the occupancies converged to 0.37(3) Ag/0.40(5) Zn in M1a, 0.03(3) Ag/0.21(5) Zn in M1b, 0.90(2) Ag/0.09(2) Zn in M2, and 0.69(2) Ag/0.31(3) Zn in M3; these values correspond to the formula " $Sr_2Ag_{1.99(3)}Zn_{1.01(5)}As_3$ ". (For comparison, a refinement performed without charge restraint led to the formula

“ $\text{Sr}_2\text{Ag}_{2.02(3)}\text{Zn}_{0.96(5)}\text{As}_3$ ”). Because the amount of Ag in the M1b site is essentially zero (within standard uncertainty), this site was assumed to contain exclusively Zn atoms in the final refinement. The final difference electron density map is featureless with  $(\Delta\rho)_{\text{max}} = 4.74 \text{ e } \text{Å}^{-3}$  and  $(\Delta\rho)_{\text{min}} = -3.19 \text{ e } \text{Å}^{-3}$ . For the Eu-containing crystal, the occupancies converged to 0.18(4) Ag/0.03(7) Zn in M1a, 0.23(5) Ag/0.62(7) Zn in M1b, 0.67(2) Ag/0.33(3) Zn in M2, and 0.94(2) Ag/0.06(3) Zn in M3 if the charge constraint is applied. Because the M1a site is clearly disfavored from being occupied by Zn atoms, it was restricted to contain only Ag atoms. With this modification to the model and the charge restraint applied, the occupancies converged to 0.18(1) Ag in M1a, 0.28(2) Ag/0.55(3) Zn in M1b, 0.66(2) Ag/0.34(3) Zn in M2, and 0.93(2) Ag/0.08(3) Zn in M3, resulting in the formula “ $\text{Eu}_2\text{Ag}_{2.05(2)}\text{Zn}_{0.97(3)}\text{As}_3$ ”. However, inspection of the difference map ( $(\Delta\rho)_{\text{max}} = 11.11 \text{ e } \text{Å}^{-3}$  and  $(\Delta\rho)_{\text{min}} = -4.76 \text{ e } \text{Å}^{-3}$ ) revealed residual electron density at a 2c site (0, 0, 1/2) which is located in the center of an octahedron with M1b and M2 atoms at a distance of  $\sim 2.6 \text{ Å}$ . At this stage, we recognized that  $\text{Eu}_2\text{Ag}_2\text{ZnAs}_3$  is isostructural to  $\text{Yb}_2\text{Zn}_3\text{Ge}_{3.1}$ , in which a similar void centered in an octahedron of Zn atoms is partially occupied (0.192(6)) by Ge atoms.<sup>25</sup> On the basis of this precedent, As atoms were placed in this site (labeled as As4) and only isotropic displacement parameters were introduced; the occupancy converged to 0.19(1), and  $U_{\text{iso}}$  was 0.047(4)  $\text{Å}^2$  at this stage. This feature appears to be peculiar to this structure type, but it is curious that the Sr analogue does not suffer from it. Equally large displacements of the corresponding partially occupied Ge4 site are also observed in  $\text{Yb}_2\text{Zn}_3\text{Ge}_{3.1}$  and could not be eliminated by attempts to refine in lower symmetry space groups ( $C_m$  or  $C_2$ ).<sup>25</sup> Although it was possible to apply an additional restraint such that the sum of the occupancies over the four As sites corresponds to 3 atoms per formula unit, the main As sites did not stray far from full occupancy (0.98–0.99), so we fixed their occupancies to unity in the final refinement. The final formula  $\text{Eu}_2\text{Ag}_{2.03(2)}\text{Zn}_{0.98(3)}\text{As}_{3.08(1)}$  deviates from charge balance slightly, in which the excess As atoms introduce additional filled As states that would lower the Fermi energy below the pseudogap in a semiconducting or semimetallic material. For simplicity, we refer to the ideal stoichiometric formulas ( $\text{A}_2\text{Ag}_2\text{ZnAs}_3$  with the  $\text{Yb}_2\text{Zn}_3\text{Ge}_3$ -type structure) in subsequent discussion.

Atomic positions were standardized with the program STRUCTURE TIDY.<sup>26</sup> Final values of the positional and displacement parameters are given in Table 2, and selected interatomic distances are listed in Table 3. Further data, in the form of crystallographic information files (CIFs), are available as Supporting Information or may be obtained from Fachinformationszentrum Karlsruhe, Abt. PROKA, 76344 Eggenstein-Leopoldshafen, Germany (Nos. CSD-424028, 424029, 424030, 424031).

**Electrical Resistivity Measurements.** Single crystals of  $\text{Sr}_2\text{Zn}_2\text{As}_3$  and  $\text{Eu}_2\text{Zn}_2\text{As}_3$  were mounted for standard four-probe electrical resistivity measurements along the needle axis (corresponding to the crystallographic  $b$  axis) on a Quantum Design Physical Property Measurement System (PPMS) equipped with an ac transport controller (model 7100). The current was 100  $\mu\text{A}$ , and the frequency was 16 Hz. Measurements were conducted twice on separate crystals for each compound. Corresponding crystals of  $\text{Sr}_2\text{Ag}_2\text{ZnAs}_3$  and  $\text{Eu}_2\text{Ag}_2\text{ZnAs}_3$  were unfortunately too small to permit resistivity measurements.

**Band Structure Calculations.** Tight-binding linear muffin tin orbital band structure calculations were performed on

**Table 2. Atomic Coordinates and Equivalent Isotropic Displacement Parameters for  $\text{A}_2\text{Zn}_2\text{As}_3$  and  $\text{A}_2\text{Ag}_2\text{ZnAs}_3$  (A = Sr, Eu)<sup>a</sup>**

atom	occupancy	x	y	z	$U_{\text{eq}}$ ( $\text{Å}^2$ ) <sup>b</sup>
$\text{Sr}_2\text{Zn}_2\text{As}_3$					
Sr1	1	0.26694(3)	0	0.66409(4)	0.0071(1)
Sr2	1	0.39248(3)	0	0.04821(4)	0.0077(1)
Zn1	1	0.03802(4)	0	0.31432(5)	0.0085(1)
Zn2	1	0.41130(4)	0	0.34890(5)	0.0089(1)
As1	1	0.07517(3)	0	0.12467(4)	0.0073(1)
As2	1	0.15194(3)	0	0.79726(4)	0.0068(1)
As3	1	0.38920(3)	0	0.54186(4)	0.0064(1)
$\text{Eu}_2\text{Zn}_2\text{As}_3$					
Eu1	1	0.26674(2)	0	0.66429(3)	0.0073(1)
Eu2	1	0.39395(2)	0	0.05022(3)	0.0080(1)
Zn1	1	0.04012(5)	0	0.31430(6)	0.0091(1)
Zn2	1	0.41019(5)	0	0.34714(6)	0.0095(1)
As1	1	0.07743(4)	0	0.12487(5)	0.0074(1)
As2	1	0.15341(4)	0	0.80033(5)	0.0073(1)
As3	1	0.38709(4)	0	0.54008(5)	0.0070(1)
$\text{Sr}_2\text{Ag}_2\text{ZnAs}_3$					
Sr1	1	0.26175(4)	0	0.66880(5)	0.0095(1)
Sr2	1	0.44099(4)	0	0.10312(5)	0.0113(1)
M1a	0.40(2) Ag, 0.35(3) Zn	0.0264(1)	0	0.3682(2)	0.0225(4)
M1b	0.26(1) Zn	0.0428(4)	0	0.3421(6)	0.0225(4)
M2	0.91(2) Ag, 0.09(2) Zn	0.41384(4)	0	0.36119(5)	0.0212(2)
M3	0.69(2) Ag, 0.31(2) Zn	0.22920(4)	0	0.09685(5)	0.0148(2)
As1	1	0.08173(4)	0	0.11695(6)	0.0128(1)
As2	1	0.16187(5)	0	0.82799(6)	0.0128(1)
As3	1	0.38125(4)	0	0.54630(6)	0.0115(1)
$\text{Eu}_2\text{Ag}_2\text{ZnAs}_3$					
Eu1	1	0.26115(3)	0	0.66851(4)	0.0068(1)
Eu2	1	0.43479(3)	0	0.09285(4)	0.0074(1)
M1a	0.18(1) Ag	0.0368(6)	0	0.3624(7)	0.0215(6)
M1b	0.29(2) Ag, 0.54(3) Zn	0.0513(1)	0	0.3321(2)	0.0215(6)
M2	0.65(2) Ag, 0.35(3) Zn	0.41989(6)	0	0.36080(9)	0.0279(4)
M3	0.91(2) Ag, 0.09(3) Zn	0.22310(5)	0	0.09835(7)	0.0140(2)
As1	1	0.08121(6)	0	0.11964(8)	0.0068(2)
As2	1	0.15421(8)	0	0.81922(11)	0.0128(2)
As3	1	0.37865(7)	0	0.53993(9)	0.0105(2)
As4	0.17(1)	0	0	1/2	0.053(6)

<sup>a</sup>All atoms are in Wyckoff position 4i in space group  $C2/m$ , except for As4 in  $\text{Eu}_2\text{Ag}_2\text{ZnAs}_3$ , which is in Wyckoff position 2c. <sup>b</sup> $U_{\text{eq}}$  is defined as one-third of the trace of the orthogonalized  $U_{ij}$  tensor.

$\text{Sr}_2\text{Zn}_2\text{As}_3$  and  $\text{Sr}_2\text{Ag}_2\text{ZnAs}_3$  within the local density and atomic spheres approximation with use of the Stuttgart TB-LMTO-ASA program (version 4.7).<sup>27</sup> The basis sets included Sr 4d/4f/5s/5p, Zn 3d/4s/4p, and As 3d/4s/4p orbitals with the Sr 4f/5p and As 4d orbitals being downfolded. Integrations in reciprocal space were carried out with an improved tetrahedron method over 172 irreducible  $k$  points within the first Brillouin zone. For  $\text{Sr}_2\text{Ag}_2\text{ZnAs}_3$ , six ordered models were examined in which either the M1a or M1b site and both the M2 and M3 sites are each fully occupied by different permutations of one Zn and two Ag atoms per formula unit.

**Table 3.** Selected Interatomic Distances (Angstroms) in  $A_2Zn_2As_3$  and  $A_2Ag_2ZnAs_3$  (A = Sr, Eu)

	$Sr_2Zn_2As_3$	$Eu_2Zn_2As_3$
A1–As3	3.0808(8)	3.0468(8)
A1–As2	3.0859(8)	3.0664(8)
A1–As3 (×2)	3.1089(7)	3.0614(7)
A1–As1 (×2)	3.1387(7)	3.0966(7)
A2–As2 (×2)	3.1742(7)	3.1390(7)
A2–As2	3.2195(9)	3.1709(9)
A2–As1 (×2)	3.2247(7)	3.1924(7)
A2–As1 (×2)	3.3128(8)	3.2958(8)
Zn1–As2	2.5304(10)	2.5402(11)
Zn1–As3 (×2)	2.5530(6)	2.5446(7)
Zn1–As1	2.6683(9)	2.6488(10)
Zn2–As3	2.5353(9)	2.5284(10)
Zn2–As2 (×2)	2.5602(6)	2.5507(7)
Zn2–As3	2.6775(10)	2.6788(11)
Zn2–Zn2	3.0050(12)	3.0039(14)
Zn2–Zn1 (×2)	3.1569(8)	3.1598(8)
As1–As1	2.4959(10)	2.4883(11)
	$Sr_2Ag_2ZnAs_3$	$Eu_2Ag_2ZnAs_3$
A1–As3	3.1389(8)	3.0980(9)
A1–As3 (×2)	3.1691(6)	3.1186(7)
A1–As1 (×2)	3.2315(6)	3.2210(6)
A1–As2	3.2393(8)	3.1744(9)
A2–As1 (×2)	3.1788(6)	3.1587(7)
A2–As2 (×2)	3.2276(6)	3.1716(7)
A2–As1 (×2)	3.3340(7)	3.2772(7)
M1a–As3 (×2)	2.5554(7)	2.525(3)
M1a–As2	2.5661(13)	2.551(7)
M1b–As3 (×2)	2.526(2)	2.5663(10)
M1b–As2	2.737(6)	2.730(2)
M1b–As1	3.183(3)	2.859(3)
M2–As3	2.6243(8)	2.6008(12)
M2–As3	2.8975(8)	2.7784(12)
M2–As2 (×2)	2.8984(5)	2.8323(8)
M3–As1	2.6266(9)	2.6534(11)
M3–As2 (×2)	2.6737(5)	2.6913(7)
M3–As2	2.7520(9)	2.7777(12)
M2–M3 (×2)	2.8195(7)	2.8090(11)
M2–M2 (×2)	2.8327(10)	2.7681(17)
M1a–M2 (×2)	2.8922(15)	2.940(7)
M1b–M2 (×2)	3.212(6)	3.264(2)
As1–As1	2.4954(11)	2.5077(16)
As4–M1b (×2)		2.596(3)
As4–M2 (×4)		2.6297(5)

## RESULTS AND DISCUSSION

**Crystal Structure.**  $Sr_2Zn_2As_3$  and  $Eu_2Zn_2As_3$  are ternary arsenides that are representatives of the recently identified  $Ba_2Cd_2Sb_3$ -type structure,<sup>20</sup> whereas  $Sr_2Ag_2ZnAs_3$  and  $Eu_2Ag_2ZnAs_3$  are quaternary arsenides adopting the unusual  $Yb_2Zn_3Ge_3$ -type structure.<sup>25</sup> The building block common to both series of arsenides is a fragment characteristic of the  $CaAl_2Si_2$ -type structure.<sup>10</sup> In  $AM_2X_2$  phases with the  $CaAl_2Si_2$ -type structure, the X atoms are arranged in close-packed nets in an hcp stacking with M atoms occupying all tetrahedral sites and A atoms occupying all octahedral sites within alternating pairs of nets. A one-dimensional ribbon of four chains of edge-sharing  $MA_4$  tetrahedra is excised to give the fragments found in  $A_2Zn_2As_3$  and  $A_2Ag_2ZnAs_3$  (A = Sr, Eu) (Figure 1).

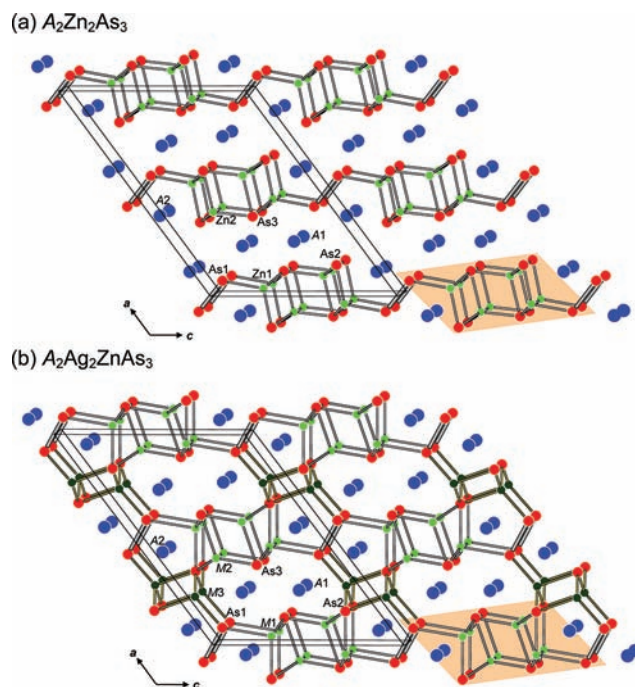


**Figure 1.** Structures of (a)  $A_2Zn_2As_3$  and (b)  $A_2Ag_2ZnAs_3$  (A = Sr, Eu) viewed down the  $b$  direction. Large blue circles are A atoms, small green circles are M (= Ag, Zn) atoms, and medium red circles are As atoms. Bonds to the interstitial M3 sites in  $A_2Ag_2ZnAs_3$  are shown in yellow.  $CaAl_2Si_2$ -type fragments are highlighted in orange.

In  $A_2Zn_2As_3$ , these ribbons extend along the  $b$  direction and are connected by As1–As1 bonds (2.49 Å) along the  $c$  direction, resulting in anionic  $[Zn_2As_3]^{4-}$  layers parallel to the  $bc$  plane. The  $A^{2+}$  cations reside in two kinds of sites: A1 with octahedral geometry is found between the layers as in  $CaAl_2Si_2$ , and A2 with more irregular geometry (CN5 + 2) is nestled closely to the As1–As1 bonds within the layers. The structural relationship is more than just a formal one because  $AZn_2As_2$  phases (A = Sr, Eu) with the  $CaAl_2Si_2$ -type structure do exist.<sup>7,8</sup> For example, comparison of metrical details shows that the octahedrally coordinated Sr and tetrahedrally coordinated Zn atoms undergo only slight distortions on proceeding from  $SrZn_2As_2$  (Sr–As, 3.128(1) Å; As–Sr–As, 84.93(3)°; Zn–As, 2.549(1)–2.606(3) Å; As–Zn–As, 111.83(5)°)<sup>7</sup> to  $Sr_2Zn_2As_3$  (Sr1–As, 3.0808(8)–3.1387(7) Å; As–Sr1–As, 85.86(2)–94.31(2)°; Zn–As, 2.530(1)–2.678(1) Å; As–Zn–As, 102.32(2)–113.95(2)°).

In  $A_2Ag_2ZnAs_3$ , there are  $[M_2As_3]$  layers parallel to the  $bc$  plane similar to the ones found in  $A_2Zn_2As_3$  but they are connected together along the  $a$  direction to form a three-dimensional structure when interstitial M3 sites with tetrahedral geometry are occupied. This condensation partitions the interlayer space formerly in  $A_2Zn_2As_3$  into a larger oblong tunnel outlined by a 12-membered ring (formed by two fused heptagons) occupied by A1 atoms and a smaller pentagonal tunnel occupied by A2 atoms. The unit cell volume increases slightly (by  $\sim 60$  Å<sup>3</sup>) on progressing from  $A_2Zn_2As_3$  to  $A_2Ag_2ZnAs_3$ , but this expansion occurs more along the  $a$  axis (by 0.4 Å) than the  $b$  and  $c$  axes (by 0.2 Å). Although the A and As sites remain essentially intact in this structural evolution, the M sites exhibit disorder of Ag and Zn atoms and undergo significant distortions, as shown within the  $CaAl_2Si_2$ -type fragment (Figure 2a). The M1 site is split into two, both of

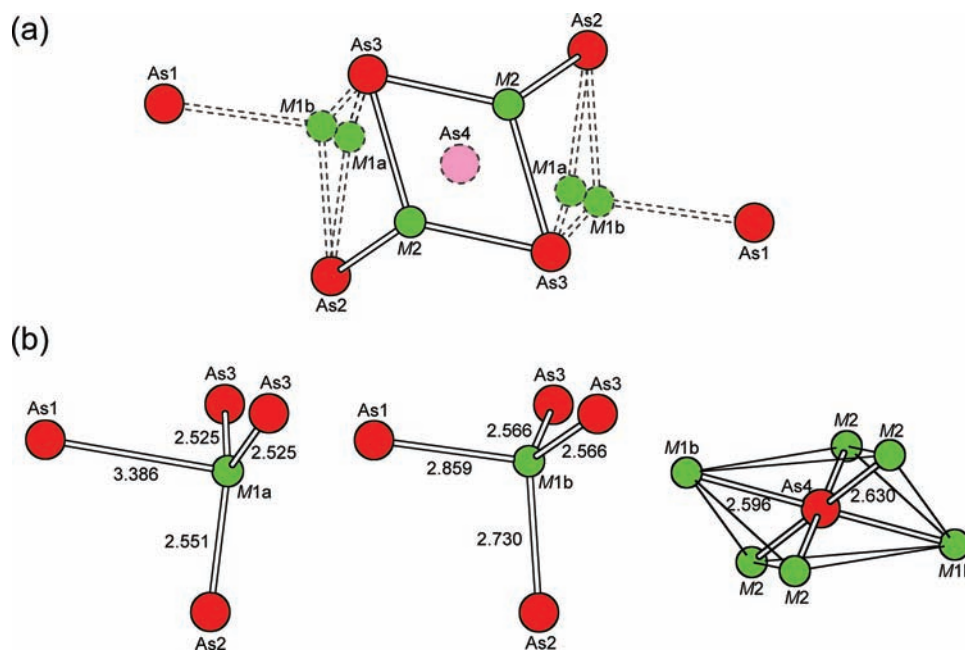


**Figure 2.** (a) Further details on the disordered M1 and M2 sites within the  $\text{CaAl}_2\text{Si}_2$ -type fragments found in  $\text{A}_2\text{Ag}_2\text{ZnAs}_3$  ( $\text{A} = \text{Sr}, \text{Eu}$ ). Partially occupied As4 site is found only in  $\text{Eu}_2\text{Ag}_2\text{ZnAs}_3$ . (b) Coordination environments around M1a, M2a, and As4 sites, with bond distances shown for  $\text{Eu}_2\text{Ag}_2\text{ZnAs}_3$ .

which are displaced away from ideal tetrahedral coordination: M1a has only three close As neighbors (2.5–2.6 Å) and is nearly in a regular trigonal planar geometry, whereas M1b could be perhaps better described to be in a trigonal pyramidal geometry (2.5–2.7 Å) given that the fourth As atom is markedly more distant (2.8–3.2 Å) (Figure 2b). The site preferences for the Ag and Zn atoms (Table 2) are complex and difficult to rationalize. Simple size and electronegativity considerations dictate that smaller sites should be preferred by smaller atoms, whereas sites with lower CN should be preferred by more electronegative atoms. Because Ag is larger than Zn (cf. Pauling metallic radii of 1.34 Å for Ag and 1.21 Å for Zn),<sup>28</sup> it occupies the M2 site preferentially, which has the longest average distances to neighboring As atoms (~2.8 Å). At the same time, Ag is also more electronegative than Zn (cf. Pauling electronegativities of 1.93 for Ag and 1.65 for Zn).<sup>28</sup> However, the M1a site, which has the lowest CN, contains a mixture of nearly equal proportions of Ag and Zn atoms in  $\text{Sr}_2\text{Ag}_2\text{ZnAs}_3$ , whereas it contains only Ag atoms in  $\text{Eu}_2\text{Ag}_2\text{ZnAs}_3$ . This observation suggests that the A component in  $\text{Sr}_2\text{Ag}_2\text{ZnAs}_3$  vs  $\text{Eu}_2\text{Ag}_2\text{ZnAs}_3$  may exert an indirect influence, through matrix effects, on the site preferences of the Ag and Zn atoms. A further distinction between these two compounds is that  $\text{Eu}_2\text{Ag}_2\text{ZnAs}_3$  contains a partially occupied (17%) As4 site within the center of an octahedron formed by the M atoms in the  $\text{CaAl}_2\text{Si}_2$ -type fragment (Figure 2). This site also appears in the parent  $\text{Yb}_2\text{Zn}_3\text{Ge}_{3.1}$ -type structure, filled with Ge atoms at a similar occupancy (19%).<sup>25</sup>

**Electronic Structure.** The bonding in  $\text{A}_2\text{Zn}_2\text{As}_3$  and  $\text{A}_2\text{Ag}_2\text{ZnAs}_3$  is readily rationalized from the charge-balanced formulations,  $(\text{A}^{2+})_2(\text{Zn}^{2+})_2(\text{As}^{2-})(\text{As}^{3-})_2$  and  $(\text{A}^{2+})_2(\text{Ag}^+)_2(\text{Zn}^{2+})(\text{As}^{2-})(\text{As}^{3-})_2$ , respectively, obtained by applying the Zintl concept. The As1 atoms are not fully reduced and must thus share electrons to complete their octets, resulting in the As1–As1 dimers. Substitution of two  $\text{Ag}^+$  ions in  $\text{A}_2\text{Zn}_2\text{As}_3$  with one  $\text{Zn}^{2+}$  ion maintains the same electron count in  $\text{A}_2\text{Ag}_2\text{ZnAs}_3$ . All atoms attain closed-shell electron configurations,

and these compounds should be small band gap semiconductors. To confirm this prediction, electrical resistivity measurements were performed on  $\text{A}_2\text{Zn}_2\text{As}_3$ , for which sufficiently large single crystals could be obtained. The temperature dependence of the electrical resistivity for  $\text{Sr}_2\text{Zn}_2\text{As}_3$  does reveal semiconducting behavior with a small intrinsic band gap of 0.037 eV obtained by fitting the data to the equation  $\ln \sigma = \ln \sigma_0 - (E_g/2kT)$  (Figure 3a). In contrast,  $\text{Eu}_2\text{Zn}_2\text{As}_3$  is quite different. The temperature dependence of the electrical resistivity between 125 and 300 K actually has a slightly positive slope indicative of metallic behavior (Figure 3b). When the temperature is decreased below 125 K, the resistivity rises rapidly to a sharp peak at 25 K and then drops abruptly. A band gap of 0.015 eV is obtained from fitting the data in the region between 25 and 50 K if thermally activated behavior is assumed. An explanation for this resistivity transition can be traced to the interaction of conduction electrons with f electrons on  $\text{Eu}^{2+}$  species undergoing magnetic ordering. Unfortunately, the phase purity of the  $\text{Eu}_2\text{Zn}_2\text{As}_3$  sample was not acceptable enough to permit magnetic measurements. However, there is a strong resemblance to the resistivity behavior of other Eu-containing Zintl phases, such as  $\text{EuM}_2\text{Pn}_2$  ( $\text{M} = \text{Ga}, \text{In}; \text{Pn} = \text{P}, \text{As}$ )<sup>29–31</sup> and  $\text{Ca}_{14-x}\text{Eu}_x\text{MnSb}_{11}$ ,<sup>32</sup> as well as to the metal–insulator transition seen in  $\text{EuO}$ ,<sup>33</sup> for which mechanisms involving ferromagnetic ordering of  $\text{Eu}^{2+}$  have been frequently proposed.

Electronic structure calculations were carried out to help answer two major questions: (1) How does the band structure evolve on progressing from  $\text{Sr}_2\text{Zn}_2\text{As}_3$  to  $\text{Sr}_2\text{Ag}_2\text{ZnAs}_3$ , and what are the implications if the electron count is changed? (2) What is the preferred site distribution of Ag and Zn atoms in  $\text{Sr}_2\text{Ag}_2\text{ZnAs}_3$ ? The density of states (DOS) and crystal orbital Hamilton population (COHP) curves for  $\text{Sr}_2\text{Zn}_2\text{As}_3$  (Figure 4a) resemble those for  $\text{Ba}_2\text{Cd}_2\text{Pn}_3$  ( $\text{Pn} = \text{As}, \text{Sb}$ ).<sup>20</sup> The interpretation of the band structure is aided by inspecting the atomic orbital projections of the DOS (Figure S4a in Supporting Information). A valence band is separated from a conduction

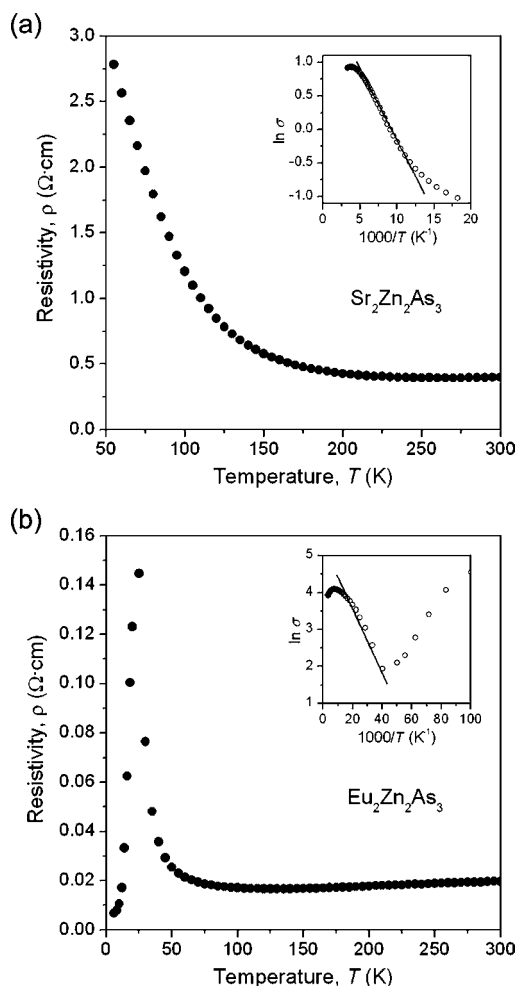


**Figure 3.** Plots of electrical resistivity vs temperature for (a)  $\text{Sr}_2\text{Zn}_2\text{As}_3$  and (b)  $\text{Eu}_2\text{Zn}_2\text{As}_3$ . (Insets) Plots of the natural logarithm of the electrical conductivity vs inverse temperature.

band by a gap of 0.2 eV, somewhat larger than the experimental value of 0.04 eV determined from the electrical resistivity measurement. The valence band splits into two subbands corresponding to Zn 4s states contributing to the lower energy one (from  $-5.5$  to  $-4.3$  eV) and Zn 4p states to the higher energy one (from  $-4.3$  to 0 eV) with mixing of As 4p states throughout the entire range. Not shown to even lower energy are narrow bands of essentially localized states corresponding to further Zn 3d and As 4s/4p states. Although Sr-based states dominate the empty conduction band above the Fermi level, there is a substantial contribution of Sr 5d states to the valence band as well; this cation–anion orbital mixing implies that the assumption of innocent  $\text{Sr}^{2+}$  ions derived from the Zintl concept is not quite accurate. Inspection of the COHP curves that at the electron count for  $\text{Sr}_2\text{Zn}_2\text{As}_3$  ( $43 e^-$  per formula unit) Sr–As bonding levels are filled and continue to be available above the Fermi level, Zn–As bonding is just optimized with all bonding and no antibonding levels filled, and As–As bonding remains substantial with all bonding and just a few antibonding levels filled. The spike in the As–As COHP curve near  $-3.5$  eV can be traced to bonding character provided by the  $\sigma_g(2p)$  molecular orbital of the As1–As1 dimer.

On progressing to  $\text{Sr}_2\text{Ag}_2\text{ZnAs}_3$ , there are two significant changes to the band structure (Figure 4b). First, insertion of a third metal site (M3, assumed to be occupied solely by Ag atoms)

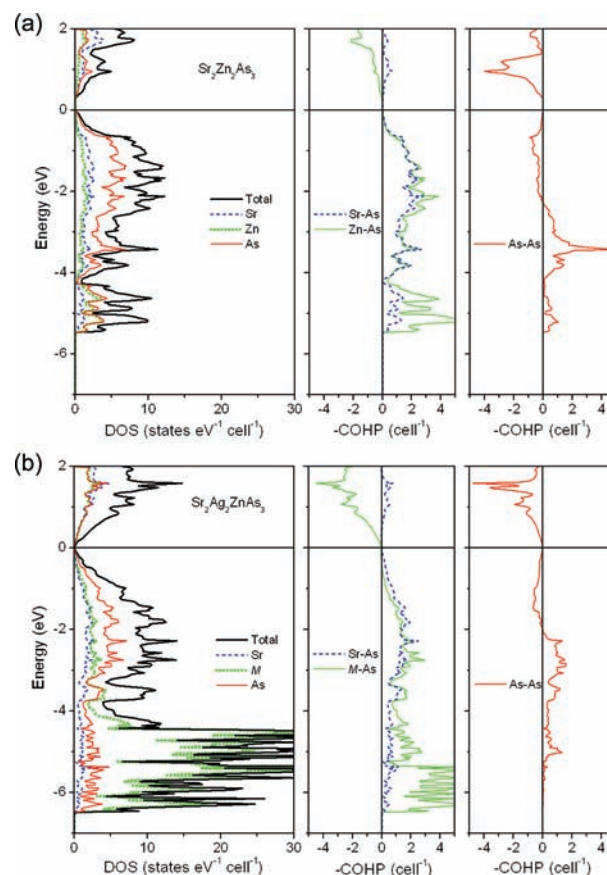


**Figure 4.** Band structures of (a)  $\text{Sr}_2\text{Zn}_2\text{As}_3$  and (b)  $\text{Sr}_2\text{Ag}_2\text{ZnAs}_3$  (model 1). Left panels show the density of states (DOS) and their atomic projections; middle and right panels show the crystal orbital Hamiltonian population (–COHP) curves for Sr–As, M–As, and As–As contacts. The horizontal line at 0 eV marks the Fermi level.

introduces additional Ag-based 4d states in the region from  $-6.5$  to  $-5.5$  eV to the DOS (as seen by inspection of Figure S4b in Supporting Information). Table 4 compares the integrated COHP

**Table 4.** Comparison of –ICOHP Values in  $\text{Sr}_2\text{Zn}_2\text{As}_3$  and  $\text{Sr}_2\text{Ag}_2\text{ZnAs}_3$

contact	–ICOHP (eV bond $^{-1}$ )	–ICOHP (eV cell $^{-1}$ )	contribution (%)
$\text{Sr}_2\text{Zn}_2\text{As}_3$			
Sr–As	0.58	7.56	34.8
Zn–As	1.43	11.47	52.9
As–As	2.66	2.66	12.3
$\text{Sr}_2\text{Ag}_2\text{ZnAs}_3$			
Sr–As	0.47	5.68	26.3
M–As	1.21	13.35	61.7
As–As	2.59	2.59	12.0

values for  $\text{Sr}_2\text{Zn}_2\text{As}_3$  and  $\text{Sr}_2\text{Ag}_2\text{ZnAs}_3$ , showing that M–As contacts provide the majority of the bonding population, followed by Sr–As and As–As contacts. Although the Sr–As and M–As contacts weaken slightly in  $\text{Sr}_2\text{Ag}_2\text{ZnAs}_3$  (as indicated by the –ICOHP values per bond), there are now a greater number of M–As contacts such that they dominate the bonding in the structure. The orbitals of the inserted M3 atoms also interact with those of the As1–As1 dimer, such that the spike at  $-3.5$  eV previously seen in the As–As COHP curve in

$\text{Sr}_2\text{Zn}_2\text{As}_3$  becomes attenuated. Second, the valence band widens in energy dispersion such that the band gap separating it from the conduction band vanishes. This transition to semimetallic behavior permits the electron count to be able to deviate slightly from  $53 e^-$  per formula unit as seen in related compounds, either as an increase in  $\text{Eu}_2\text{Ag}_2\text{ZnAs}_{3.1}$  ( $53.5 e^-$ ) or as a decrease in  $\text{Yb}_2\text{Zn}_3\text{Ge}_{3.1}$  ( $52.4 e^-$ ), if a rigid band model is assumed. Within the small energy range corresponding to these electron counts around the Fermi level the COHP curves do not change very rapidly. For example, in  $\text{Yb}_2\text{Zn}_3\text{Ge}_{3.1}$ , the decrease in electron count lowers the Fermi level to  $-0.7 \text{ eV}$ , at which point the weakening of Sr–As and M–As bonding is counteracted by the strengthening of As–As bonding, as antibonding As–As levels are depopulated. The Ge1–Ge1 distance of  $2.505 \text{ \AA}$  in  $\text{Yb}_2\text{Zn}_3\text{Ge}_{3.1}$  is just  $0.02 \text{ \AA}$  longer than the sum of the Pauling metallic radii ( $2.48 \text{ \AA}$ ),<sup>25,28</sup> whereas the nearly identical As1–As1 distance of  $2.495 \text{ \AA}$  in  $\text{Sr}_2\text{Ag}_2\text{ZnAs}_3$  is  $0.08 \text{ \AA}$  longer than the sum of the radii ( $2.42 \text{ \AA}$ ).

The distribution of Ag and Zn atoms into several available metal sites (M1a, M1b, M2, and M3) is an interesting feature in  $\text{Sr}_2\text{Ag}_2\text{ZnAs}_3$ , posing what is known as a “coloring problem”.<sup>34–36</sup> The band structure of the ternary compound  $\text{Sr}_2\text{Zn}_2\text{As}_3$  was first examined to determine which of the two sites, M1 (unsplit) and M2, would be preferred to be occupied by Ag atoms if they were to substitute for Zn atoms. The expectation is that the site with the higher QVAL values, which measure the integrated electron density within the Wigner-Seitz sphere around a given site, should be preferred by the more electronegative Ag atoms. The QVAL is barely higher (11.43) for M1 than for M2 (11.32), indicating only a slight preference of the Ag atoms to occupy the former. This prediction is inconsistent with the experimental results for  $\text{Sr}_2\text{Ag}_2\text{ZnAs}_3$  (Table 3), probably because it fails to take into account that the M1–As bond lengths would be too short ( $2.5\text{--}2.6 \text{ \AA}$ ) and assumes that the  $\text{Sr}_2\text{Zn}_2\text{As}_3$  host structure would remain undistorted. Several models of  $\text{Sr}_2\text{Ag}_2\text{ZnAs}_3$  were then considered in which Ag and Zn atoms occupy the metal sites in alternative distributions (Table 5). The key conclusion is that

**Table 5. Relative Total Energy for Different Models of  $\text{Sr}_2\text{Ag}_2\text{ZnAs}_3$**

model	M1a	M1b	M2	M3	$E_{\text{tot}}$ (eV cell <sup>-1</sup> )
1	Zn		Ag	Ag	0.330
2	Ag		Zn	Ag	0.841
3	Ag		Ag	Zn	0.556
4		Zn	Ag	Ag	0
5		Ag	Zn	Ag	0.856
6		Ag	Ag	Zn	0.577

the two lowest energy models are the ones in which Zn atoms occupy either the M1a or the M1b site and the Ag atoms occupy both the M2 and M3 sites, in agreement with the observed site preferences. Of course, competing against this energy minimization is the tendency toward entropy maximization, which would favor random mixing of the Ag and Zn atoms among these sites.

## CONCLUSIONS

Preparation of the quaternary arsenides  $\text{A}_2\text{Ag}_2\text{ZnAs}_3$ , derived from the ternary host arsenides  $\text{A}_2\text{Zn}_2\text{As}_3$ , illustrates that the ideas of aliovalent substitution and stuffing of interstitial sites

serve as robust strategies for targeting new solid-state structures. However, prediction of the more subtle features of these structures, such as site preferences, remains challenging. Notwithstanding their significant differences in size and electronegativity, the Ag and Zn atoms exhibit partial disorder within multiple sites. The disappearance of the band gap in  $\text{A}_2\text{Ag}_2\text{ZnAs}_3$  suggests that the electron count and thus the electronic properties could be modified by varying the proportion of Ag and Zn atoms. These arsenides appear to possess many of the desirable characteristics required for a good thermoelectric material, and it would be worthwhile undertaking further measurements of their physical properties.

## ASSOCIATED CONTENT

### Supporting Information

X-ray crystallographic files in CIF format, powder XRD patterns, and an SEM image. This material is available free of charge via the Internet at <http://pubs.acs.org>.

## AUTHOR INFORMATION

### Corresponding Author

\*E-mail: [arthur.mar@ualberta.ca](mailto:arthur.mar@ualberta.ca).

## ACKNOWLEDGMENTS

The Natural Sciences and Engineering Research Council of Canada and the University of Alberta supported this work. We thank Ms. De-Ann Rollings (Department of Earth and Atmospheric Sciences) for assistance with the EDX analysis.

## REFERENCES

- (1) Kauzlarich, S. M.; Brown, S. R.; Snyder, G. J. *Dalton Trans.* **2007**, 2099–2107.
- (2) Toberer, E. S.; May, A. F.; Snyder, G. J. *Chem. Mater.* **2010**, *22*, 622–634.
- (3) Rotter, M.; Tegel, M.; Johrendt, D. *Phys. Rev. Lett.* **2008**, *101*, 107006–1–107006–4.
- (4) Mandrus, D.; Sefat, A. S.; McGuire, M. A.; Sales, B. C. *Chem. Mater.* **2010**, *22*, 715–723.
- (5) Canfield, P. C.; Bud'ko, S. L. *Annu. Rev. Condens. Matter Phys.* **2010**, *1*, 27–50.
- (6) Klüfers, P.; Mewis, A. Z. *Naturforsch., B: Anorg. Chem., Org. Chem.* **1977**, *32*, 753–756.
- (7) Mewis, A. Z. *Naturforsch., B: Anorg. Chem., Org. Chem.* **1980**, *35*, 939–941.
- (8) Klüfers, P.; Neumann, H.; Mewis, A.; Schuster, H.-U. Z. *Naturforsch., B: Anorg. Chem., Org. Chem.* **1980**, *35*, 1317–1318.
- (9) Zwiener, G.; Neumann, H.; Schuster, H.-U. Z. *Naturforsch., B: Anorg. Chem., Org. Chem.* **1981**, *36*, 1195–1197.
- (10) Klüfers, P.; Mewis, H. Z. *Kristallogr.* **1984**, *169*, 135–147.
- (11) Artmann, A.; Mewis, A.; Roepke, M.; Michels, G. Z. *Anorg. Allg. Chem.* **1996**, *622*, 679–682.
- (12) Nateprov, A.; Cisowski, J.; Heimann, J.; Mirebeau, I. J. *Alloys Compd.* **1999**, *290*, 6–9.
- (13) Schellenberg, I.; Pfannenschmidt, U.; Eul, M.; Schwickert, C.; Pöttgen, R. Z. *Anorg. Allg. Chem.* **2011**, *637*, 1863–1870.
- (14) Klüfers, P.; Mewis, A. Z. *Naturforsch., B: Anorg. Chem., Org. Chem.* **1978**, *33*, 151–155.
- (15) Hellmann, A.; Löhken, A.; Wurth, A.; Mewis, A. Z. *Naturforsch., B: J. Chem. Sci.* **2007**, *62*, 155–161.
- (16) Saparov, B.; Bobev, S. *Inorg. Chem.* **2010**, *49*, 5173–5179.
- (17) Wang, J.; Yang, M.; Pan, M.-Y.; Xia, S.-Q.; Tao, X.-T.; He, H.; Darone, G.; Bobev, S. *Inorg. Chem.* **2011**, *50*, 8020–8027.
- (18) Wilson, D. K.; Saparov, B.; Bobev, S. Z. *Anorg. Allg. Chem.* **2011**, *637*, 2018–2025.
- (19) Saparov, B.; Bobev, S. *Acta Crystallogr., Sect. E: Struct. Rep. Online* **2010**, *66*, i24.

- (20) Saparov, B.; He, H.; Zhang, X.; Greene, R.; Bobev, S. *Dalton Trans.* **2010**, 39, 1063–1070.
- (21) Nientiedt, A. T.; Lincke, H.; Rodewald, U. Ch.; Pöttgen, R.; Jeitschko, W. Z. *Naturforsch., B: J. Chem. Sci.* **2011**, 66, 221–226.
- (22) Stoyko, S. S.; Mar, A. J. *Solid State Chem.* **2011**, 184, 2360–2367.
- (23) Stoyko, S. S.; Mar, A. *Inorg. Chem.* **2011**, 50, 11152–11161.
- (24) Sheldrick, G. M. *SHELXTL*, version 6.12; Bruker AXS Inc.: Madison, WI, 2001.
- (25) Grytsiv, A.; Kaczorowski, D.; Rogl, P.; Tran, V.; Godart, C.; Gofryk, K.; Giester, G. *J. Phys.: Condens. Matter* **2005**, 17, 385–397.
- (26) Gelato, L. M.; Parthé, E. *J. Appl. Crystallogr.* **1987**, 20, 139–143.
- (27) Tank, R.; Jepsen, O.; Burkhardt, A.; Andersen, O. K. *TB-LMTO-ASA Program*, version 4.7; Max Planck Institut für Festkörperforschung: Stuttgart, Germany, 1998.
- (28) Pauling, L. *The Nature of the Chemical Bond*, 3rd ed.; Cornell University Press: Ithaca, NY, 1960.
- (29) Jiang, J.; Kauzlarich, S. M. *Chem. Mater.* **2006**, 18, 435–441.
- (30) Goforth, A. M.; Klavins, P.; Fettingner, J. C.; Kauzlarich, S. M. *Inorg. Chem.* **2008**, 47, 11048–11056.
- (31) Goforth, A. M.; Hope, H.; Condrón, C. L.; Kauzlarich, S. M.; Jensen, N.; Klavins, P.; MaQuilon, S.; Fisk, Z. *Chem. Mater.* **2009**, 21, 4480–4489.
- (32) Kim, H.; Olmstead, M. M.; Klavins, P.; Webb, D. J.; Kauzlarich, S. M. *Chem. Mater.* **2002**, 14, 3382–3390.
- (33) Arnold, M.; Kroha, J. *Phys. Rev. Lett.* **2008**, 100, 046404–1–046404–4.
- (34) Miller, G. J. *Eur. J. Inorg. Chem.* **1998**, 523–526.
- (35) Misra, S.; Miller, G. J. *J. Am. Chem. Soc.* **2008**, 130, 13900–13911.
- (36) Yao, J.; Lyutyy, P.; Mozharivskyj, Y. *Dalton Trans.* **2011**, 40, 4275–4283.